

Numerical studies of offshore performance of floating protective barriers in waves and currents

MARINE 2021

Alexander Knysh^{1,*}, Jackson Coyle¹, Judson DeCew², Andrew Drach³,

M. Robinson Swift¹, Igor Tsukrov¹

¹ The University of New Hampshire, Durham, NH 03861, USA

² HALO Maritime Defense Systems, Newton, NH 03858, USA

³ The University of Texas at Austin, Austin, TX 78712, USA

* Corresponding author: Alexander Knysh, alex.knysh.u@gmail.com

ABSTRACT

Finite element modeling was applied to evaluate the performance of Triton® floating protective barrier designed by HALO Maritime Defense Systems (US) and used to provide essential protection to critical governmental, commercial, and private assets vulnerable to water-borne intrusion, such as liquefied natural gas terminals, tankers, etc. The numerical model created with Hydro-FE software was validated by physical tests and field deployment observations. Physical tests of a scaled barrier model were conducted in Chase Ocean Engineering Laboratory wave tank at the University of New Hampshire to measure response of the structure and its mooring to different single-frequency waves directed parallel and normal to the model. The field deployment of the full-scale barrier performed south-southwest of White Island, Isles of Shoals, New Hampshire, provided information on its dynamic behavior under monitored environmental conditions. Good correspondence between numerical, physical and field studies was observed. The validated numerical model of the barrier was then used to investigate its performance and seaworthiness in other current and wave conditions with different mooring pretension scenarios.

Keywords: finite element analysis, floating barriers, fluid-structure interaction, wave response.

NOMENCLATURE

$B(f)$	Bretschneider or incident wave spectrum [$\text{m}^2 \text{Hz}^{-1}$]
C_a	Added mass coefficient [-]
C_d	Normal drag coefficient [-]
C_t	Tangential drag coefficient [-]
$E(f)$	Energy density spectrum or response spectrum [$\text{m}^2 \text{Hz}^{-1}$]
\mathbf{F}	Vector of force exerted by fluid on a solid body [N]
f_m	Modal frequency [Hz]
$H_{1/3}$	Significant wave height [m]
\mathbf{u}	Vector of fluid velocity [m/s]
\mathbf{v}	Vector of body velocity [m/s]
ρ_w	Ocean water density [kg m^{-3}]
RAO	Response amplitude operator

1. INTRODUCTION

Protective barriers are used to protect naval bases, offshore platforms, ports, nuclear power facilities, bridges, dams, refineries and desalination plants and other assets from terrorist attacks in different marine environments. They prevent attacks by a simple boat loaded with explosives which is one of the most popular and dangerous types of the attack due to its relative cheapness and technical simplicity (Hill, 2009). In order to effectively prevent such catastrophes, the performance of floating protective barriers of different designs are usually investigated through field studies (DeCew and Rowell, 2013; Kalinski *et al.*, 2014). Although most of the studies have been focused on actual waterborne craft impact testing and corresponding design optimizations which are then proved by U.S. Navy and military or civilian customers (Nixon *et al.*, 2004, 2005; Bishop, 2013; Osienski *et al.*, 2017), some numerical investigations have also been conducted since large-scale tests are quite expensive and labor-intensive. For instance, a series of full-scale finite element simulations and the corresponding real impact tests of FOXX barriers were performed by Polish Naval Academy (Kiciński *et al.*, 2019). To the best of the authors' knowledge, there are no other publicly available publications related to either physical or numerical testing of floating protective barriers.

In offshore deployments, in addition to impact protection, the floating barriers and their mooring systems have to be able to withstand high energy environmental loading conditions without experiencing significant damage or even failure. The purpose of this paper is to present a comprehensive approach to the prediction and evaluation of floating barrier offshore performance using the example of a Triton® floating barrier manufactured by HALO Maritime Defense Systems, USA (Fig. 1). The approach includes a combination of full-scale field studies, scaled physical testing and numerical modeling. The four-month-long field deployment of the barrier continued from January to May 2018 near the Isles of Shoals, New Hampshire, USA, and covered a period of the winter storms. The scaled physical testing (1:20) was conducted in the University of New Hampshire (UNH) wave/tow tank (Knysh *et al.*, 2021) utilizing techniques previously developed and validated for various offshore aquaculture installations (Fredriksson *et al.*, 2000; DeCew *et al.*, 2005; Wang *et al.*, 2015). The numerical modeling was performed with the finite element analysis software Hydro-FE based on the well-validated Aqua-FE program developed at UNH (Gosz *et al.*, 1996; Tsukrov *et al.*, 2000, 2003; Fredriksson *et al.*, 2003) and extensively applied in the marine aquaculture field (DeCew *et al.*, 2010; Wang *et al.*, 2015; Knysh *et al.*, 2020). Materials of this paper are based on the approach developed in (Knysh *et al.*, 2021), with the addition of new results on barrier's response to typical and extreme North Atlantic environmental conditions (Tsukrov *et al.*, 2000; Fredriksson *et al.*, 2004) at different barrier orientations and bridle line pretensions.



Figure 1. The Triton® barrier being towed to the University of New Hampshire offshore research site on January 10, 2018.

2. PROTECTIVE BARRIER AND ITS NUMERICAL MODEL

The investigated Triton® barrier system consists of four 15 m units. Each unit is 6 m high, 3.3 m wide and stands approximately 3 m off the water. The units are joined together by dual ethylene propylene diene monomer (EPDM) rubber hinges allowing the segments to contour waves and absorb the loading due to the high energy marine environment. Schematics of a single unit as well as the barrier mooring setup can be seen in Fig. 2. Units consist of two longitudinal pipes connected to transverse and side members with upper and lower pipes, all made of high-density polyethylene (HDPE). Most of the side and transverse members are attached to the longitudinal, upper and lower pipes by butt-fusing Tees which are held in place by pins and tabs. Attachment methods also include hangers strapped around the pipe and eyes through-bolted to the pipe. The stainless steel impact netting is suspended from the upper pipe and attached to the transverse members. The first unit of the barrier deployed in the field study also included an instrument box with accelerometer and data pack powered by a solar panel. The instrument box is attached to the upper pipe that is supported by side members.

The longitudinal pipes of neighboring units are connected by hinges at the waterline and additionally secured by limiter cables that ensure structural integrity even if hinge is damaged. Longitudinal pipes contain closed cell foam flotation whereas the lower pipe is filled with heavy chain ballast providing increased stability. The impact netting of each unit is connected to each other by the net joint and placed between the longitudinal and upper pipes, so it is present along the whole barrier.

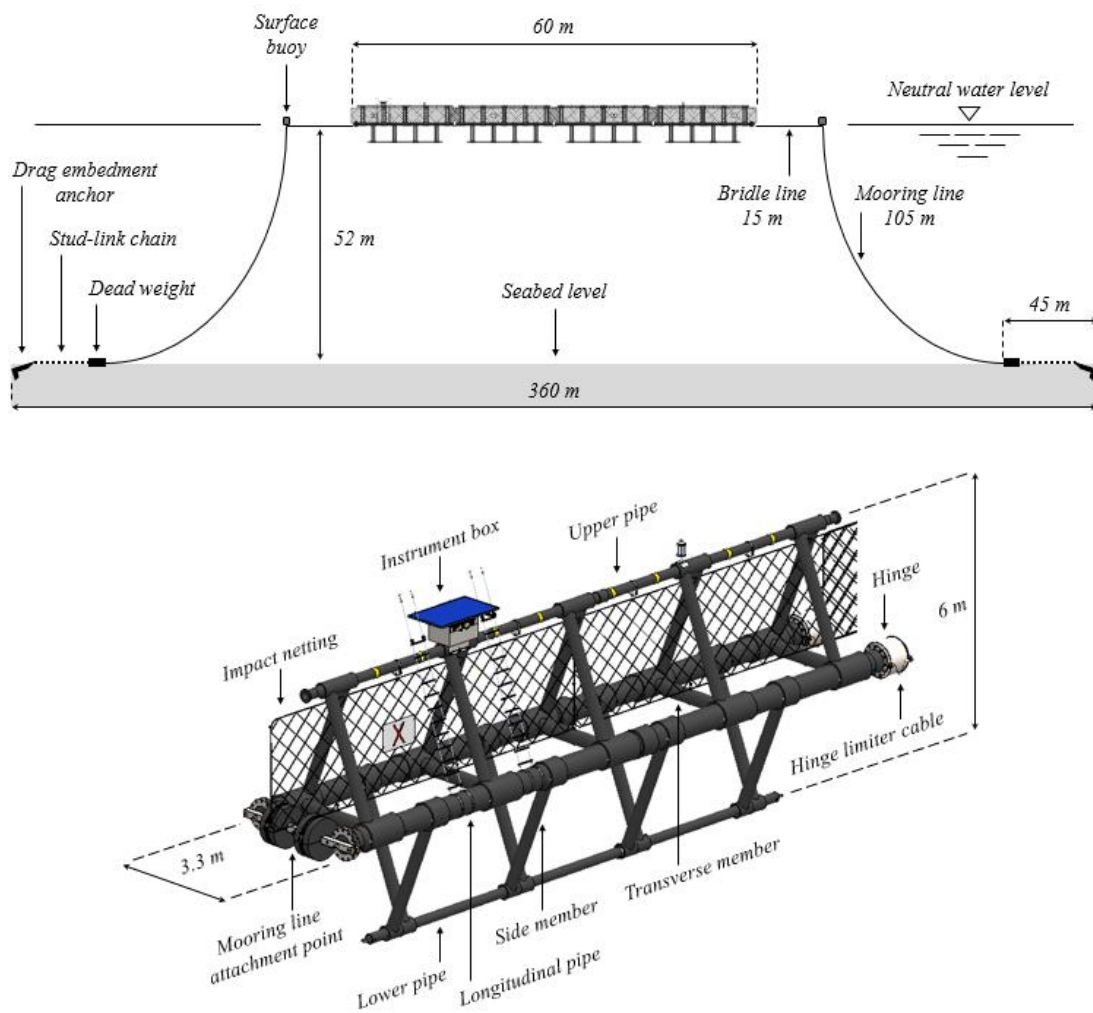


Figure 2. Schematics of the HALO Triton® barrier. The mooring setup is not to scale.

The finite element (FE) model of the full-scale barrier was created in Hydro-FE software (Fig. 3). Hydro-FE modernizes the approach previously implemented in the well-validated Aqua-FE program developed at the University of New Hampshire (Gosz *et al.*, 1996; Tsukrov *et al.*, 2000; Fredriksson *et al.*, 2003) to analyze partially or completely submerged flexible structures in the marine environment. The code is written in FORTRAN and uses the commercially available nonlinear finite element solver MSC.Marc with the graphical user interface MSC.Mentat (<https://www.mscsoftware.com/>). Wave environmental conditions in Hydro-FE are implemented using Airy wave theory (Dean and Dalrymple, 1991).

For the Triton® barrier simulations, the finite element solver was prescribed a large strain case, implicit dynamic transient operator (single-step Houbolt) and lumped mass matrices. The total load case time of 500 s with the adaptive time stepping resulted in 15,000-20,000 increments per simulation.

As the main structural components, such as longitudinals, hinges, side members, transverse members, upper and lower pipes, are not only the major source of drag and inertia forces but also important in providing structural rigidity, these components were modeled with 2-node three-dimensional beam elements to account for bending moments and torque. At the same time, mooring chain, bridle and mooring lines were modeled with 2-node three-dimensional truss elements to preserve their compliance. Basic material and geometrical properties of the finite elements are given in Tab. 1.

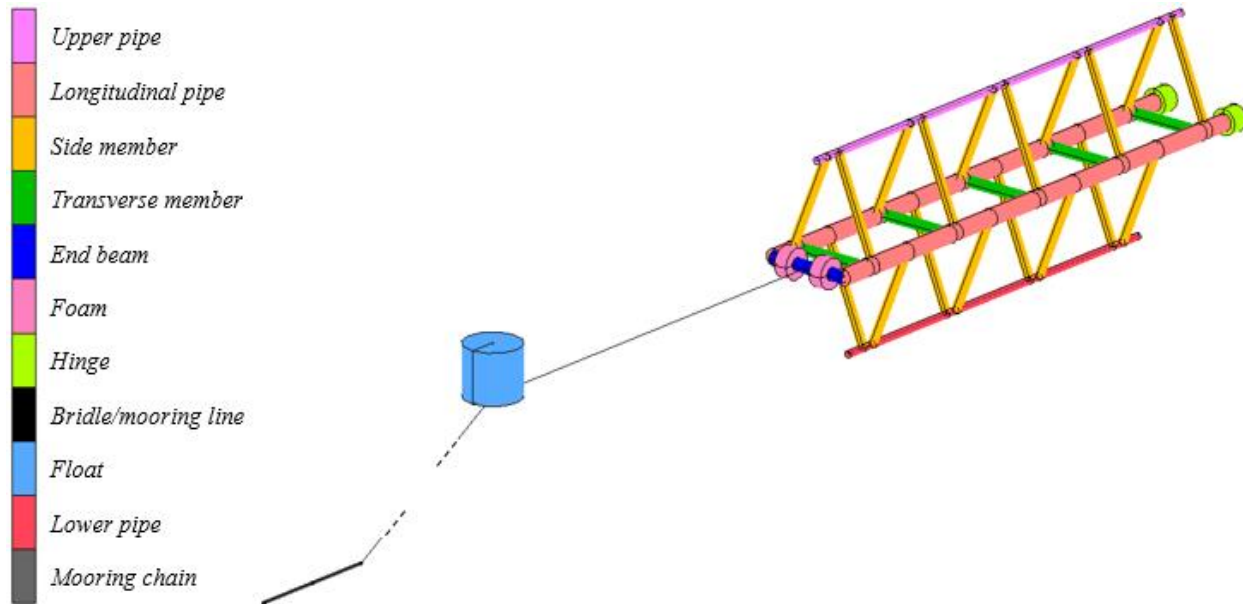


Figure 3. Finite element model of the barrier's unit and mooring system. Not to scale.

Note that most of the finite element parameters correspond to the actual properties of the barrier. However, some of them were recalculated based on reasonable simplifications as follows. The weight of small components that cannot be properly modeled (tabs, bolts, impact net, etc.) was uniformly distributed along the longitudinals, side and transverse members, hinges, upper and lower pipes. The weight of the ballast chain was added to the weight of lower pipes. Material density of floats was averaged across the whole floats' volume, whereas their Young's modulus and Poisson's ratio were selected as generic plastic values, since they do not significantly influence the overall barrier response. The diameter of the mooring chain elements was calculated to keep the chain density and overall weight unchanged.

Table 1. Structural and geometrical parameters of the barrier's FE model. Recalculated values are shown with gray background.

Structural component	Material density [kg/m ³]	Young's modulus [GPa]	Poisson's ratio [-]	Flexural rigidity [MPa·m ⁴]	Cross-section area [m ²]	Outer diameter [m]	Number of elements [-]	Element type
Longitudinal	962	1.07	0.41	1.37	0.045	0.508	120	2-node, beam
Hinge	n/a	n/a	n/a	n/a	n/a	n/a	6	2-node, beam
Side member	962	1.07	0.41	0.115	0.013	0.273	72	2-node, beam
Transverse member	962	1.07	0.41	0.320	0.027	0.324	20	2-node, beam
Upper pipe	962	1.07	0.41	0.066	0.012	0.219	44	2-node, beam
Lower pipe	4660	1.07	0.41	0.066	0.012	0.219	36	2-node, beam
Bridle/mooring line	1400	8.30	0.28	-	0.0016	0.045	134	2-node, truss
Surface float	421	1.00	0.30	-	2.2	1.676	2	2-node, truss
Mooring chain	7860	205	0.29	-	0.007	0.094	50	2-node, truss

In order to calculate force exerted by waves on structural components, the so-called Morison's equation approach (Morison *et al.*, 1950) expanded to the case of a moving cylinder (Goodman and Breslin, 1976) was used in this study. According to this approach, there are two vectors associated with each differential section dL of the submerged cylindrical body of outside diameter d_o arbitrarily moving in the water: the local fluid velocity vector \mathbf{u} and the body velocity vector \mathbf{v} . Both of these vectors can be projected on normal (perpendicular to the cylinder axis) and tangential (parallel to the cylinder axis) directions. Then, the normal projection of the force exerted on a differential section dL is

$$d\mathbf{F}_n = \rho_w \frac{\partial \mathbf{u}_n}{\partial t} dV + C_a \rho_w \left(\frac{\partial \mathbf{u}_n}{\partial t} - \frac{\partial \mathbf{v}_n}{\partial t} \right) dV + \frac{1}{2} C_d \rho_w |\mathbf{u}_n - \mathbf{v}_n| (\mathbf{u}_n - \mathbf{v}_n) dA, \quad (1)$$

where \mathbf{u}_n and \mathbf{v}_n are the normal projections of fluid and body velocities associated with section dL , C_a is the added mass coefficient, C_d is the normal drag coefficient, $dV = \frac{1}{4} \pi d_o^2 dL$ is the differential volume of section dL , and $dA = d_o dL$ is the differential normal projected area of section dL . The tangential component of the drag force is taken in the form:

$$d\mathbf{F}_t = \frac{\pi}{2} C_t \rho_w |\mathbf{u}_t - \mathbf{v}_t| (\mathbf{u}_t - \mathbf{v}_t) dA, \quad (2)$$

where C_t is the tangential drag coefficient, \mathbf{u}_t and \mathbf{v}_t are the tangential projections of fluid and body velocities associated with differential section dL . In this numerical study, all of the barrier components were assumed to be smooth cylinders and assigned normal drag coefficient, tangential drag coefficient and added mass coefficient of $C_d = 1.2$, $C_t = 0.01$, $C_a = 1$, respectively.

3. NUMERICAL LOAD CASES

Three stages of the barrier testing were conducted. First two stages, scaled single-frequency wave tank test and full-scale field study, served to validate the numerical model (Knysh *et al.*, 2021), while third stage was purely numerical and aimed to examine the performance of the barrier in typical and extreme North Atlantic conditions.

Both scaled physical (1:20) and numerical single-frequency wave tests were conducted for two model orientations: inline and sideways (Fig. 4). Seven wave frequencies and three different wave heights were investigated; however high frequency large waves could not be achieved due to the wave tank physical limitations. A full list of waves successfully produced by the Chase Ocean Engineering Laboratory wave tank and recalculated to full-scale is presented in Tab. 2. Wave frequencies chosen for the single-frequency tests are in the range from 0.1 Hz to 0.3 Hz which spans the range for which there is sufficient wave energy to excite a response from the barrier. The numerical model was additionally validated in several free-release tests (Knysh *et al.*, 2021).

Table 2. Single-frequency wave testing parameters investigated in UNH wave maker. The values are recalculated to full-scale.

Wave frequency [Hz]	0.099	0.111	0.127	0.149	0.178	0.223	0.298
Wave period [s]	10.101	9.009	7.874	6.711	5.617	4.484	3.355
Wave height [m]	1, 2, 3	1, 2, 3	1, 2, 3	1, 2, 3	1, 2, 3	1, 2	1

In the field study, both the heave response energy density and the wave forcing Bretschneider spectra were obtained for a representative offshore data set recorded at the 52 m deep UNH research site located 2.8 km south-southwest from White Island, Isles of Shoals, New Hampshire, US, from 3:36 am to 4:00 am on April 5, 2018 (Knysh *et al.*, 2021). As the energy density spectrum required vertical motion of the barrier as a function of time, the corresponding vertical acceleration data was double integrated over time. The NDBC station at Jeffrey's Ledge provided values of the significant wave height (2.04 m) and the modal wave frequency (0.13 Hz) needed to calculate the Bretschneider wave spectrum. The same approach, in terms of the energy density spectrum, was used for the random waves numerical simulation. However, the Bretschneider wave spectrum considered in the field study was discretized and implemented in Hydro-FE as a superposition of 22 single-frequency waves in the frequency range from 0.10 Hz to 0.30 Hz .

The influence of typical and extreme environmental conditions (Tsukrov *et al.*, 2000; Fredriksson *et al.*, 2004), bridle line pretensions and barrier orientations on the overall barrier dynamic response are also numerically investigated in this paper. The typical conditions consisted of 1.2 m wave height, 7 s wave period, 76 m wave length and 0.25 m/s of current tidal component, which is typical for 55 m deep site south of the Isles of Shoals, New Hampshire. The extreme loading conditions were represented by 9 m wave height, 8.8 s wave period, 120 m

wave length with 1 m/s current since the maximum current at the site do not exceed this value. Bridle line pretensions of 2224 N (500 lbf) and 4448 N (1000 lbf) were tested for three different orientations: inline/parallel or 0° , sideways/perpendicular or 90° , angled or 45° . Note that current and wave propagation directions are collinear for both typical and extreme conditions.

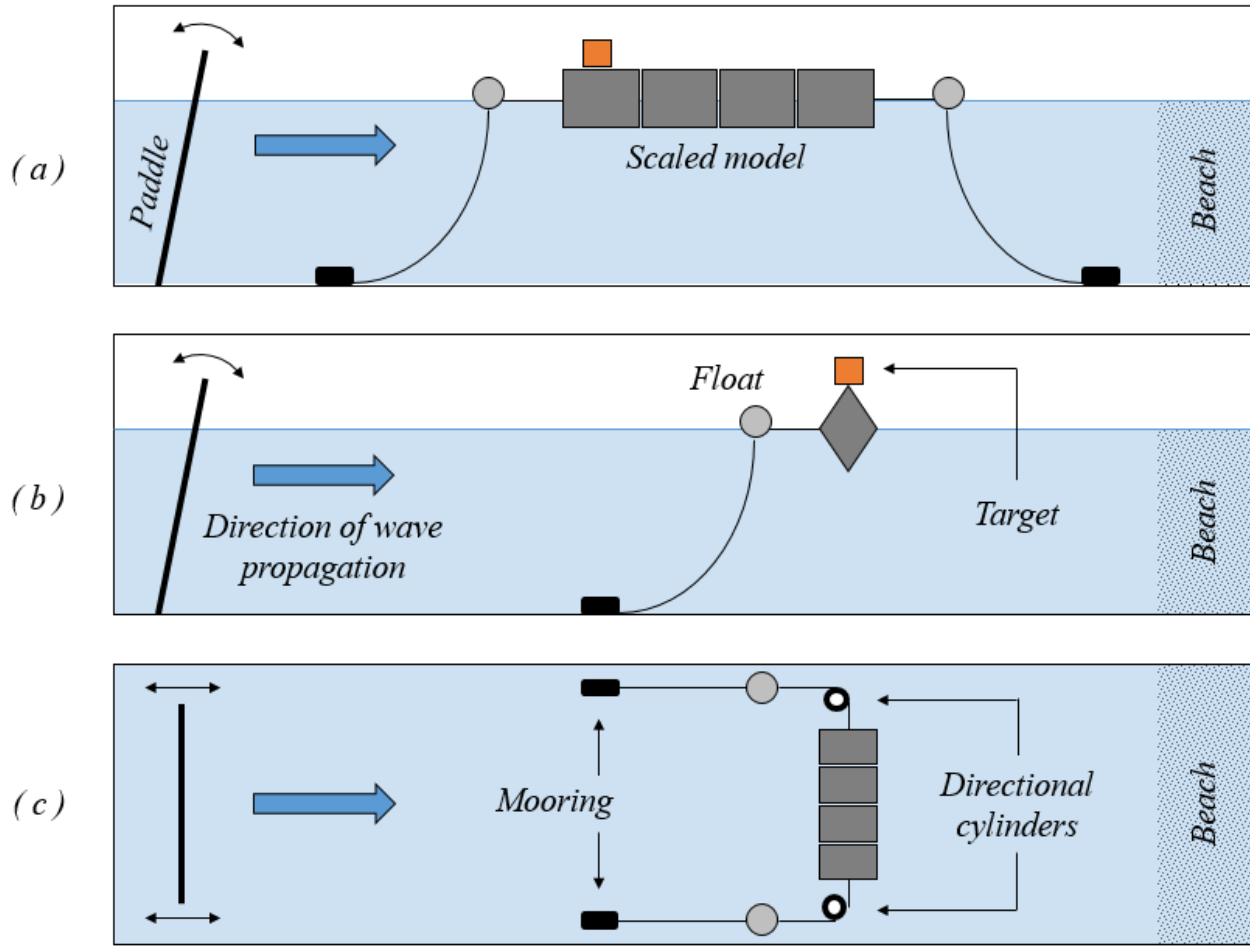


Figure 4. The UNH wave tank experimental setup: (a) inline model orientation, side view; (b) sideways model orientation, side view; (c) sideways model orientation, top view.

4. SIMULATION RESULTS AND DISCUSSION

The barrier motion and mooring line tensions resulting from single-frequency wave forcing were characterized by response amplitude operators (RAOs) common in the field of floating structures design. The heave RAO represented relative vertical motion of the barrier and was defined as

$$RAO_h = \frac{A_m}{A_w}, \quad (3)$$

where A_m is the amplitude of barrier vertical motion and A_w is the wave amplitude or half of the wave height. Pitch and roll RAOs represented angular motion of the system and were defined as

$$RAO_{\theta} = \frac{A_{\theta}}{A_w}, \quad (4)$$

where A_{θ} is the corresponding barrier's angular motion amplitude in radians. In order to analyze force factors in the system, force RAO for bridle line tension was calculated as follows:

$$RAO_f = \frac{A_f}{A_w}, \quad (5)$$

where A_f is the amplitude of bridle line tensions. It should be noted that during the processing of the load cell data, large spikes in tensions were registered at individual points in time. If the values of force in these points were more than three times the standard deviation, they were simply excluded from the data set. The load cell data was then filtered with simple moving average (SMA) technique (Brown and Mac Berthouex, 2002).

To investigate the barrier heave response to a random wave forcing and to make use of field data, the random waves heave response amplitude operator RAO_{hr} were utilized (Sethuraman and Venugopal, 2013):

$$RAO_{hr}(f) = \sqrt{\frac{E(f)}{B(f)}}, \quad (6)$$

where f is the frequency in hertz, $E(f)$ is the energy density spectrum of the barrier heave motion or response spectrum, $B(f)$ is the Bretschneider or incident wave spectrum. The Bretschneider wave spectrum was calculated as follows

$$B(f) = \frac{5}{16} \frac{H_{1/3}^2}{f_m} \left(\frac{f_m}{f}\right)^5 e^{-\frac{5}{4}\left(\frac{f_m}{f}\right)^4}, \quad (7)$$

where $H_{1/3}$ is the significant wave height, f_m is the modal (most probable) frequency of any given wave in hertz.

The comparison between heave, pitch/roll and force RAOs obtained from physical tests and numerical simulations is shown in Figs. 5-7. It can be seen in Fig. 5 that all numerical inline heave results demonstrated similar behavior: RAO remains around 1 for the lowest wave frequencies (wave length is 11 times longer than barrier unit length) with the slight increase at about 0.18 Hz and significant decline at 0.22 Hz and 0.30 Hz (wave length is about 2 and 1 barrier unit lengths, respectively). Physical testing results follow the same trend with the exception of the high frequency RAO value for the 2 m wave. For the sideways model orientation, the observed heave RAOs are mostly in the range of 0.95-1.05. However, three data points with high values of RAO can be seen for tank tests at the low wave frequencies for 2 m and 3 m waves. Subsequent investigation of the test records conducted after the tests were completed showed that the issue was caused by the shift in camera placement as the barrier clearly contoured waves with the RAO around 1. It was decided to include the initial tests results in the figure for consistency.

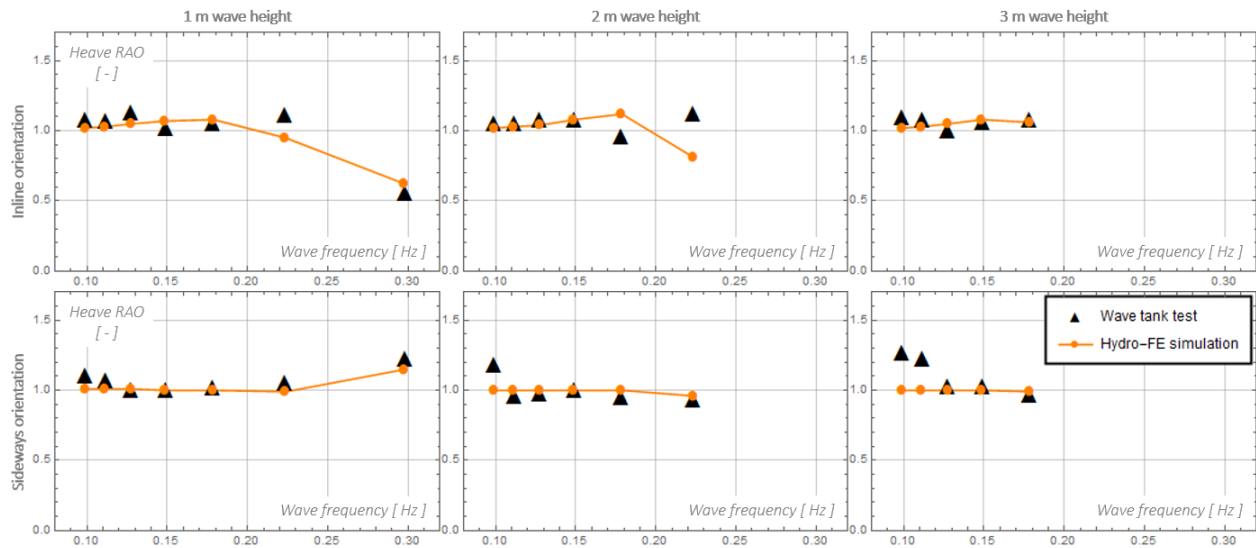


Figure 5. Full-scale heave RAO observed in physical tests and numerical simulations. The upper row of plots represents inline model orientation while the lower one represents sideways orientation. First, second and third columns correspond to 1 m , 2 m and 3 m waves, respectively.

Pitch and roll RAOs showed good agreement between physical and numerical values for both inline and sideways model orientations (Fig. 6). The inline (pitch) RAOs reach their peak of about $0.10\text{-}0.13\text{ rad/m}$ and then decay as wave length approaches 1-2 barrier unit lengths. Note that pitch RAOs reach their maximum for 1 m and 2 m waves at different frequencies. The sideways (roll) results follow the pattern of gradual increase in RAOs with wave frequency. The highest inclination angle amplitude registered among all inline tests is 8.5° , whereas for sideways tests it is less than 15.5° (Tab. 3).

Heave RAO results show that the barrier behaves as a wave follower with two exceptions of 1 m and 2 m inline waves at the highest frequencies, where heave RAO drops down (excluding one physical test). At these wave frequencies and heights, barrier does not fully contour water surface and faces upcoming waves earlier, thus reducing heave and pitch amplitudes (Fig. 6). At the same time, roll RAO consistently grows with wave frequency regardless of incident wave height. We attribute this to the wave slope increase with wave frequency while the barrier width being much smaller than wave lengths. Such behavior can result in a somewhat excessive inclination of the structure (Tab. 3) but does not influence its stability. In all of the performed tests, none have resulted in the barrier's flip or impact with an upcoming wave. All abovementioned considerations are supported by observations in the numerical and physical tests.

Table 3. The maximum inclination angle amplitude for inline and sideways model orientations among considered wave frequencies.

Frequency [Hz]	0.099	0.111	0.127	0.149	0.178	0.223	0.298
Inline test	3.60°	4.38°	5.58°	6.87°	8.50°	4.87°	1.58°
Sideways test	3.43°	4.29°	6.01°	8.59°	12.89°	15.47°	13.75°

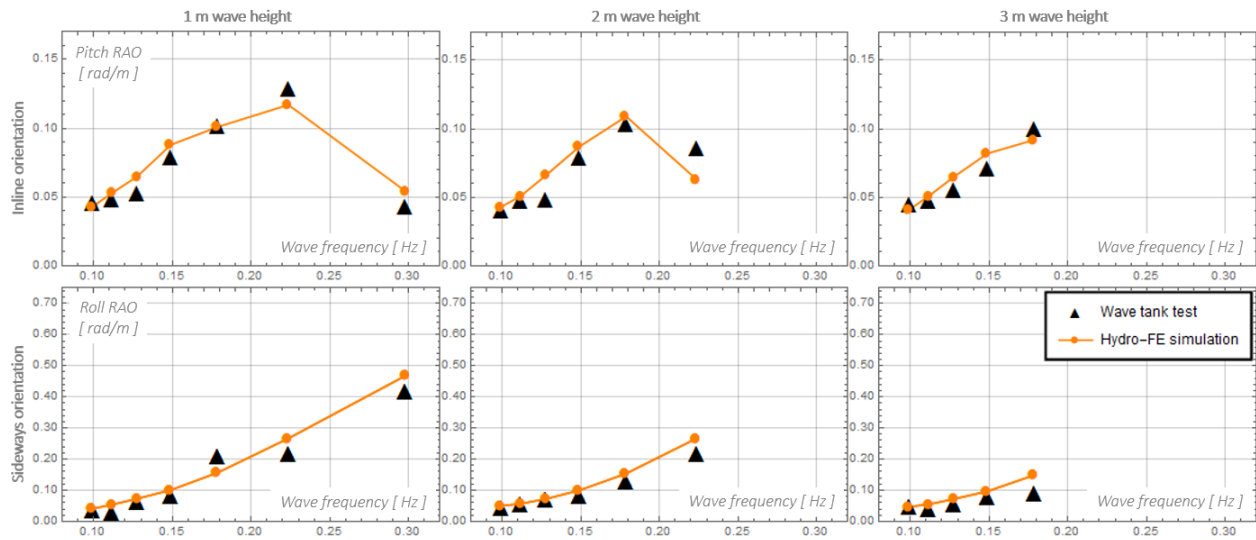


Figure 6. Full-scale pitch and roll RAO observed in physical tests and numerical simulations. The upper row of plots represents inline model orientation while the lower one represents sideways orientation. First, second and third columns correspond to 1 m, 2 m and 3 m waves, respectively.

Fig. 7 presents force RAOs obtained from numerical modeling and tank testing. Both numerical and physical test RAOs for the inline model orientation demonstrated a tendency to rise with increase of wave frequency and had a visible plateau from 0.13 Hz to 0.15 Hz. The major discrepancy is observed for 1 m waves where numerically predicted RAOs are higher than those from physical tests. In the case of sideways orientation, good correspondence between numerical models and physical tests is observed with the exception of 0.30 Hz 1 m wave.

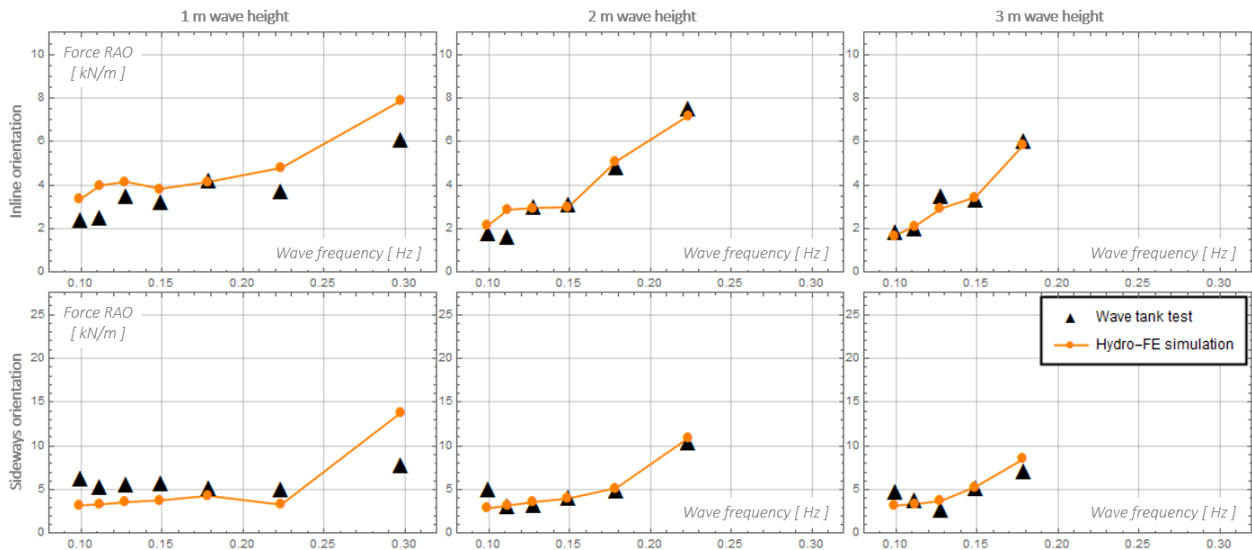


Figure 7. Full-scale force RAO observed in physical tests and numerical simulations. The upper row of plots represents inline model orientation while the lower one represents sideways orientation. First, second and third columns correspond to 1 m, 2 m and 3 m waves respectively.

The force RAO show a pronounced sensitivity to the wave loading frequency: RAO consistently trends upwards with the increase in the wave frequency. We attribute it to the minor mooring line jerking that still occurs due to

increasing wave slope and rapid change in the barrier elevation as a result. It is worth noting that the increased RAO at high frequencies is also partially attributed to the deteriorating quality of the measurement signal (increasing signal-to-noise ratio). Even though mooring chain provided reasonable damping to the mooring line, the jerking effect could not be fully eliminated because the chain itself must be heavy enough to secure barrier's position. The maximum tensions of bridle and mooring lines observed in physical and numerical testing were 42 and 35 times lower than their breaking strength, respectively, as the mooring was intentionally oversized in this test field deployment.

A comparison between incident random waves spectrum, and response spectra from filed study and numerical simulation is shown in Fig. 8. Note that the barrier was assumed to be oriented inline with the bridle line pretension of 2224 N . The correspondence between barrier response spectra is good indicating that Hydro-FE captures the essential physics of wave-barrier interaction under random waves conditions in the field. A significant dampening is observed which is attributed to the mooring system configuration: interaction effects of line pretension, shallow angle of the anchor lines and large reserve of “dead weight-chain” portion of the mooring.

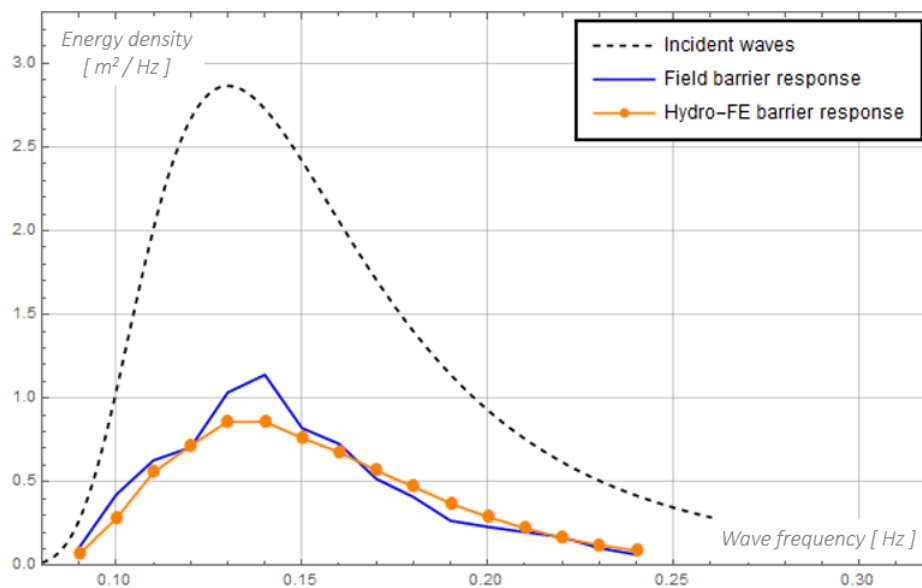


Figure 8. Energy density spectra of random waves and barrier responses in field study and Hydro-FE simulation. Random waves significant wave height is 2.04 m and modal wave frequency is 0.13 Hz .

The RAO results of the barrier numerical modeling in typical and extreme conditions for different barrier orientations and bridle line pretensions are presented in Fig. 9. While typical conditions do not demonstrate any unexpected barrier response and all values are comparable to single frequency tests, the extreme case makes a huge difference in terms of heave, pitch/roll, force RAOs and absolute values. Heave RAO of about 0.7 is achieved at the 45° orientation and none of the single-frequency tests reached such a low value since the maximum wave height was only 3 m . The sideways or 90° orientation shows quite high for 9 m waves roll RAO of about 0.06 with corresponding maximum inclination angle of 26.5° . Force RAO increases linearly with the orientation angle and almost reaches 30 kN/m which is significantly higher than any value from the wave tank tests. The corresponding maximum tensions of bridle and mooring lines were still 3 times lower than their breaking strength. Note that the effect of the pretension turned out to be negligible.

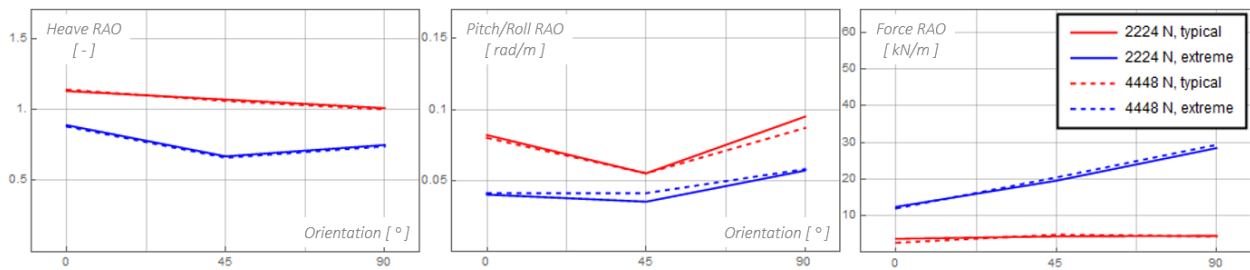


Figure 9. Heave, pitch/roll and force RAOs observed in numerical modeling of the barrier for 2224 N/4448 N pretensions and 0°/45°/90° orientations in typical and extreme conditions.

The numerical simulations and inspections of the barrier conducted during and after deployment were used to compare its performance with the design requirements. The data showed that (1) the connectors and hinges exceeded expectations in terms of dynamic performance and engineering robustness; (2) the designed hydrostatic and hydrodynamic stability of the barrier was proven to be adequate; (3) the design choice of reducing compliance variations between the structural components (pipe versus hinges) has proven to be well balanced and performed within the operational bounds; (4) the chosen level of barrier pretension provided a good balance between minimizing the barrier surface movement (“watch circle”) and alleviating end effects (snapping and oversubmerging); (5) the designed ratio of buoyancy and ballast delivered a good balance of wave following and dampening. Overall system was designed for 10 m significant wave height with the period of 12 s and has demonstrated robust performance in the operational and storm field conditions.

5. CONCLUSIONS

This paper presents a comprehensive approach to predicting and evaluating the seaworthiness of floating protective barriers and their mooring systems for deployment in high energy offshore environments. Good correspondence between the Froude-scaled physical models, numerical simulation results and field test data has been observed.

Numerical models built in the Hydro-FE finite element analysis software demonstrated their ability to reproduce most of the results observed in physical testing (with the exception of three outlier data points) and full-scale field data. Based on the modeling effort, it is recommended that mechanical and inertial contribution of small structural components of the barriers is included in the larger structural elements by assigning equivalent effective values to their density, geometric parameters and stiffness.

Successful utilization of the scaled physical models included selection of some approximate values for diameter and weight of several components due to unavailability of exactly scaled parts. The biggest challenge was implementation of the mooring system in the case of sideways tests when the direction of wave propagation was perpendicular to the barrier and the width of the tank prevented exact modeling. This challenge was overcome by a specially-built mooring arrangement utilizing smooth, vertical directional cylinders to redirect the mooring bridle along the length of the tank.

Field tests demonstrated seaworthiness and robustness of the Triton® floating barrier developed by HALO Maritime Defense Systems and provided an abundant data to develop the best deployment and inspection practices and to evaluate performance of individual barrier components, and overall system stability. The studies allowed successful validating of the numerical model and engineering approach using physical model and field data. The approach was proven to provide a good predictive capability for designing and optimizing floating barrier systems. Additional numerical tests of the validated model showed that the barrier can withstand typical and extreme North Atlantic environmental conditions.

ACKNOWLEDGEMENTS

The authors gratefully acknowledge financial support of the New Hampshire Innovation Research Center. Participation of Michael Osienski, Tom Sherwin, and Eric Rines from HALO in the field studies is greatly appreciated. We also thank Black Dog Divers for their on-site help and support. Finally, thanks to Nate Reynolds and Dave Shay for their assistance.

REFERENCES

- Bishop, J., 2013. Security barrier system. EP2627964B1.
- Brown, L., Mac Berthouex, P., 2002. Statistics for Environmental Engineers, Second Edition, Statistics for Environmental Engineers, Second Edition. <https://doi.org/10.1201/9781420056631>
- DeCew, J., Fredriksson, D.W., Bugrov, L., Swift, M.R., Eroshkin, O., Celikkol, B., 2005. A case study of a modified gravity type cage and mooring system using numerical and physical models. *IEEE J. Ocean. Eng.* 30, 47–58. <https://doi.org/10.1109/JOE.2004.841400>
- DeCew, J., Rowell, M., 2013. Hydrodynamic Analysis of the HMDS Guardian System and Sentry Buoy. Technical report.
- DeCew, J., Tsukrov, I., Risso, A., Swift, M.R., Celikkol, B., 2010. Modeling of dynamic behavior of a single-point moored submersible fish cage under currents. *Aquac. Eng.* 43, 38–45. <https://doi.org/10.1016/j.aquaeng.2010.05.002>
- Fredriksson, D.W., DeCew, J., Swift, M.R., Tsukrov, I., Chambers, M.D., Celikkol, B., 2004. The design and analysis of a four-cage grid mooring for open ocean aquaculture, in: *Aquacultural Engineering*. <https://doi.org/10.1016/j.aquaeng.2004.05.001>
- Fredriksson, D.W., Swift, M.R., Irish, J.D., Tsukrov, I., Celikkol, B., 2003. Fish cage and mooring system dynamics using physical and numerical models with field measurements. *Aquac. Eng.* [https://doi.org/10.1016/S0144-8609\(02\)00043-2](https://doi.org/10.1016/S0144-8609(02)00043-2)
- Fredriksson, D.W., Swift, M.R., Muller, E., Baldwin, K., Celikkol, B., 2000. Open ocean aquaculture engineering: System design and physical modeling. *Mar. Technol. Soc. J.* <https://doi.org/10.4031/MTSJ.34.1.5>
- Goodman, T., Breslin, J., 1976. Statics and dynamics of anchoring cables in waves. *J. Hydronautics* 10, 113–120.
- Gosz, M., Kestler, K., Swift, M.R., Celikkol, B., 1996. Finite Element Modeling of Submerged Aquaculture Net-Pen Systems. *Open Ocean Aquac. Proc. Int. Conf* 8–10.
- Hill, B.P., 2009. Maritime terrorism and the small boat attack threat to the United States: a proposed response. Naval Postgraduate School, Monterey, California.
- Kalinski, M.E., Bryson, L.S., Krumenacher, A.D., Phillips, B.T., Ethington, Z., Webster, B.T., 2014. Existing technologies for deterring and defeating waterside attack of dams. *Int. J. Crit. Infrastructures*. <https://doi.org/10.1504/IJCIS.2014.066341>

- Kiciński, R., Jurczak, W., Jabłońska, M., 2019. Technical Aspect concerning Vessels Halt Safety upon Terrorist Hazard. *J. Konbin.* <https://doi.org/10.2478/jok-2019-0030>
- Knysh, A., Coyle, J., Decew, J., Drach, A., Swift, M.R., Tsukrov, I., 2021. Floating protective barriers : Evaluation of seaworthiness through physical testing , numerical simulations and field deployment. *Ocean Eng.* 108707. <https://doi.org/10.1016/j.oceaneng.2021.108707>
- Knysh, A., Tsukrov, I., Chambers, M., Swift, M.R., Sullivan, C., Drach, A., 2020. Numerical modeling of submerged mussel longlines with protective sleeves. *Aquac. Eng.* <https://doi.org/10.1016/j.aquaeng.2019.102027>
- Morison, J.R., Johnson, J.W., Schaaf, S.A., 1950. The Force Exerted by Surface Waves on Piles. *J. Pet. Technol.* 2, 149–154. <https://doi.org/10.2118/950149-G>
- Nixon, L., Slaughter, S., Taylor, R., Seelig, W., 2005. Near shore port security barrier. US6843197B1.
- Nixon, L., Slaughter, S., Taylor, R., Seelig, W., 2004. Port security barrier system. US6681709B1.
- Osienski, M., DeCew, J., Sherwin, T., Rines, E., 2017. Open water marine barrier systems. WO2018057842A1.
- Sethuraman, L., Venugopal, V., 2013. Hydrodynamic response of a stepped-spar floating wind turbine: Numerical modelling and tank testing. *Renew. Energy.* <https://doi.org/10.1016/j.renene.2012.09.063>
- Tsukrov, I., Eroshkin, O., Fredriksson, D., Swift, M.R., Celikkol, B., 2003. Finite element modeling of net panels using a consistent net element. *Ocean Eng.* 30, 251–270. [https://doi.org/10.1016/S0029-8018\(02\)00021-5](https://doi.org/10.1016/S0029-8018(02)00021-5)
- Tsukrov, I.I., Ozbay, M., Swift, M.R., Celikkol, B., Fredriksson, D.W., Baldwin, K., 2000. Open Ocean Aquaculture Engineering: Numerical Modeling. *Mar. Technol. Soc. J.* 34, 29–40. <https://doi.org/10.4031/MTSJ.34.1.4>
- Wang, X.X., Swift, M.R., Dewhurst, T., Tsukrov, I., Celikkol, B., Newell, C., 2015. Dynamics of submersible mussel rafts in waves and current. *China Ocean Eng.* 29, 431–444. <https://doi.org/10.1007/s13344-015-0030-2>